ACS OMEGA

Open Access

http://pubs.acs.org/journal/acsodf

Article

One-Step Synthesis of Silver Nanoparticles Embedded in Biobased Polyamide 56 Nanofibers with High Antibacterial Activity

Zhen Wang, Qing Gao, Bailong Hou, Wei Wang, Liya Xu, and Wei Wang*

Cite This: *ACS Omega* 2024, 9, 19272−19281

Read Online

ACCESS | Metrics & More | Article Recommendations | Supporting Information

ABSTRACT: Embedded silver nanoparticles (Ag NPs) within nanofibers represent a highly promising alternative to common antimicrobial materials, due to the combined effective biocidal properties of Ag NPs with the biocompatibility and environmental friendliness of biobased polymers. In this study, we presented a novel one-step route to fabricate biobased polyamide 56 (PA56) nanofibers embedded with uniform Ag NPs. The process involved mixing reactive silver ammonia with PA56 solutions and then using formic acid as a reducing agent. Continuous electrospinning resulted in solvent evaporation, yielding Ag NPs highly dispersed within PA56 nanonet fibrous structures (PA56/Ag). Characterization assays confirmed the successful impregnation of Ag NPs in PA56 nanofibers, with an average size of about 32.4 nm. PA56/Ag nanofibers also displayed suitable morphology, mechanical properties, and good biocompatibility in vitro. Moreover, their antimicrobial effectiveness was evaluated against *Staphylococcus aureus* and *Escherichia coli*. Collectively, the proposed PA56/Ag nanofibers possess desirable characteristics suitable for antimicrobial applications.

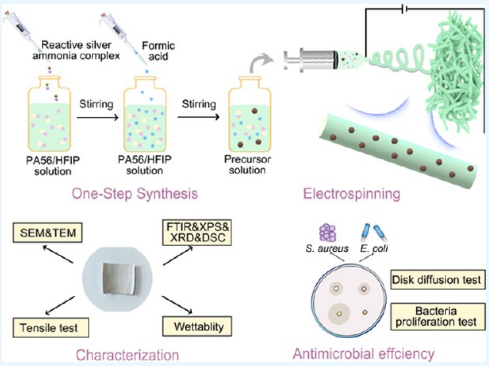

1. INTRODUCTION

Polyamide (PA), commonly known as nylon, is a key constituent of consumer products throughout industry sectors. The predominant PA products, such as PA66 and PA6, are primarily synthesized from petroleum resources, which pose significant challenges for decomposition. In response to societal concerns regarding the petroleum crisis and environmental pollution, chemical manufacturing industries are actively pursuing sustainable and eco-friendly approaches for the development of new PA products.[1,2]

Biobased PA, entirely or partially synthesized from biomass feedstocks, has emerged as an environmentally friendly alternative to petroleum-based counterparts and gained considerable traction in recent years.[3,4] Significant progress has been made in the synthesis and application of various biobased PA, including PA1010, PA610, PA510, and PA11.[5] Among these, PA56 is polymerized from renewable adipic acid and 1,5-pentanediamine, the latter of which can be commercially obtained through fermentation. This particular PA holds significant potential in textiles, biomedical applications, food packaging, and other fields, owing to its high-temperature and chemical resistance, excellent toughness, and easy processability.[5−7] Despite its promising prospects, limited studies have been conducted for the development of PA56 nanofibers, particularly for antimicrobial applications.[3,8]

Electrospinning, a simple and versatile method for producing nano- to microfiber membranes, garners attention as a viable technique for fabricating PA56 nanofibers. Due to the viscosity and thermal properties, a higher voltage (e.g., 30 kV) is necessary for the fabrication of PA56 nanofibers. Additionally, a suitable approach involves decreasing the flow rate (e.g., 0.18 mL/h) and shortening the distance between the tip and collector (e.g., 12.5 cm) in comparison to PA6 and PA66.[8] These nanofibers possess high porosity and large specific surface area, making them suitable candidates for filtration membranes, catalytic supports, energy components, electronic devices, as well as biomedicines.[9] In some cases, a variety of nanoparticles can be incorporated into nanofibers to impart new functionalities. The commonly used nanoscale components include silver (Ag), copper (Cu), copper oxide (CuO), titanium dioxide (TiO_2), zinc oxide (ZnO), and even particles composed of metal−organic frameworks (MOF).[10−13]

As a promising alternative with broad-spectrum antimicrobial activity, silver nanoparticles (Ag NPs) can release Ag^+ ions to damage the bacterial membrane and interfere with DNA/RNA replication, thereby eradicating bacteria.[14] Moreover, Ag NPs optimally regulate inflammatory responses to promote wound healing, as indicated by increased cell proliferation and wound re-epithelization.[15] However, challenges such as aggregation, cytotoxicity, and genotoxicity limit their anti-

Received: January 6, 2024
Revised: March 11, 2024
Accepted: April 9, 2024
Published: April 19, 2024

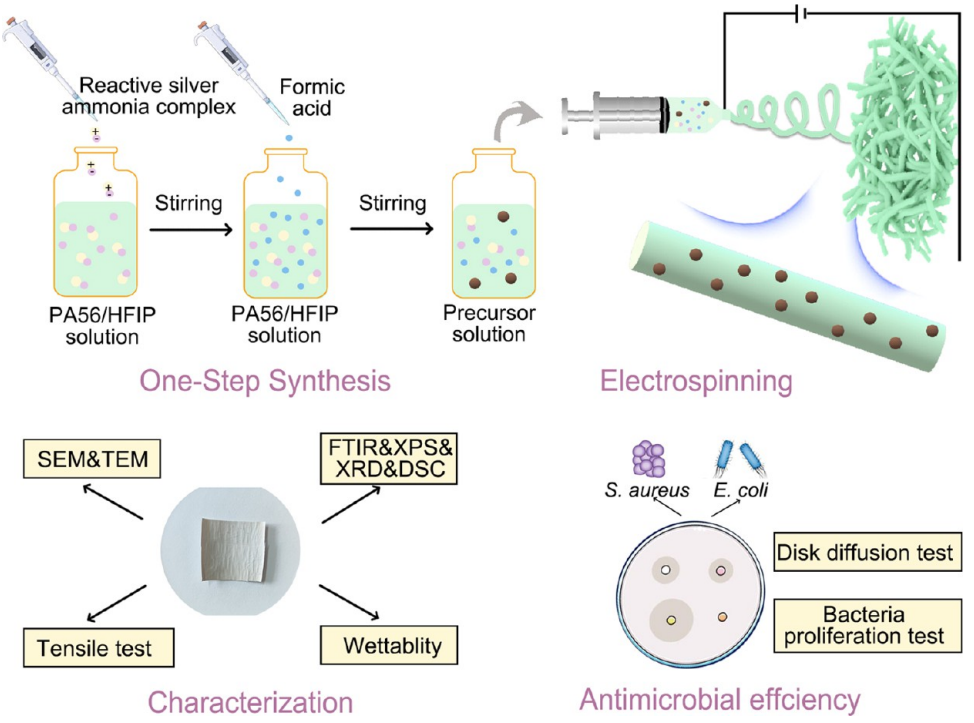

Figure 1. Schematic diagram depicting the fabrication of biobased PA56/Ag nanofibers and the investigative scheme followed in this study.

microbial efficacy. Notably, homogeneously dispersing or embedding Ag NPs inside electrospun nanofibers represents an excellent strategy for enhancing antimicrobial performance with good biocompatibility and environmental safety.[16,17] For the direct approach, the suspension of Ag NPs is added to polymer solutions for electrospinning. Avci et al. synthesized Ag NPs by *Thymus vulgaris L.* (thyme) extract reduction method, and then these Ag NPs were included in PCL/PLA nanofibers.[18] Besides, Ag NPs can deposit on nanofibers by post-treatments using thermal, ultraviolet (UV) irradiation, or chemical reduction, which require multiple steps and the use of toxic chemicals.[11,19] For example, Ag NPs synthesized with chitosan exhibited a homogeneous dispersion and high deposition on the surface of nanofibers.[20] Due to the aggregation problem and complex deposition procedure of Ag NPs, the development of a simple and environmentally friendly method for preparing nanofibers embedding Ag NPs homogeneously still remains a challenging endeavor.

In this study, we demonstrated a novel one-step route to fabricate biobased PA56 nanofibers embedded with uniform Ag NPs. The process involved mixing a complex of silver acetate and ammonium hydroxide with PA56 as the precursor solution, followed by titrating a low concentration of formic acid as the reducing agent. The continuous electrospinning facilitated solvent evaporation and the incorporation of Ag NPs into PA56 nanonet fibrous structures. The study also investigated the effect of encapsulated Ag NPs on the morphological, structural, thermal, and wettability properties of PA56/Ag nanofibers. Furthermore, the antibacterial activity was studied against Gram-negative *Escherichia coli* and Gram-positive *Staphylococcus aureus* by employing nanofibers with different Ag NP contents, in addition to the analysis of cytotoxicity and skin stimulation. Given the well-established physical, chemical, and antibacterial properties, the developed biobased PA56/Ag nanofibers might fulfill the requirements of antibacterial nanofibrous mats for wound dressings (Figure 1).

2. EXPERIMENTAL SECTION

2.1. Materials. The polyamide 56 (PA56) was kindly donated by TaiHua New Material Co., Ltd. (Zhejiang, China). Formic acid (HCOOH), hexafluoroisopropanol (HFIP), and silver acetate were obtained from Macklin Reagent (Shanghai, China). Lysogeny broth (LB) and LB agar medium plates were purchased from Hopebio (Qingdao, China). *S. aureus* (ATCC 25923) and *E. coli* (ATCC 25922) were obtained from the China General Microbiological Culture Collection Center (CGMCC). Dulbecco's modified Eagle's medium (DMEM), trypsin, and fetal bovine serum (FBS) were provided by Thermo Fisher Scientific. Cell Counting Kit-8 (CCK-8) and phosphate-buffered saline (PBS) were obtained from Yifeixue Biotechnology Co., Ltd. (Nanjing, China). BALB/3T3 clone A31 cells (3T3) were purchased from the Institute of Biochemistry and Cell Biology (Shanghai, China).

2.2. Solution Preparation and Electrospinning of PA56 Nanofibers. The biobased PA56 nanofibers were continuously fabricated using electrospinning equipment (ET-2535H, Ucalery Beijing, China). Briefly, PA56 chips were dissolved in 10 mL of HFIP and stirred overnight at room temperature to obtain a 12% (w/v) PA56 solution. It was loaded into a 5 mL standard syringe equipped with an 18G blunt stainless steel needle. Electrospinning was performed with a flow rate of 1.0 mL/h and a high voltage of 12 kV, while maintaining a 15 cm gap between the needle tip and the rotating collector. The environmental conditions inside the electrospinning setup were controlled with a relative humidity of 15−20% and a temperature range of 25−30 °C. To produce uniform nanofibrous meshes, each individual experiment was run for a duration of 4−6 h.

2.3. Fabrication of Ag NPs and PA56/Ag Nanofibers. The reactive silver ammonia complex was synthesized by vortex mixing 1 g of silver acetate into 2.5 mL of aqueous ammonium hydroxide at room temperature for 15 s.[21] The

https://doi.org/10.1021/acsomega.4c00176
ACS Omega 2024, 9, 19272−19281

complex was mixed with 10 mL of 12% PA56 solution as mentioned above, and then 10, 20, and 40 μL of HCOOH were titrated into the solution dropwise with stirring for 12 h. It changed from colorless to brown, indicating the reduction of Ag NPs. The obtained clear solutions were used for electrospinning at a flow rate of 1.0 mL/h and a high voltage of 15 kV, with a 15 cm gap between the needle tip and the rotating collector. The mass concentrations of Ag NPs in the obtained PA56/Ag nanofibers were 0.1, 0.2, and 0.4 wt %, respectively.

2.4. Characterization of PA56 and PA56/Ag Nanofibers. *2.4.1. Scanning Electron Microscopy (SEM).* The PA56/Ag nanofiber samples with varying Ag NP contents were prepared for SEM imaging. For surface morphology characterization, the samples were coated with gold using an ion sputter coater (ISC150, SuPro Instruments, China), and images were recorded by SEM (Phenom Pure, Phenom Scientific, The Netherlands) at an acceleration voltage of 5 kV. Their average diameters were determined using ImageJ software by measuring 100 individual fibers randomly, and histogram data were generated using Origin 8.0 software. Energy-dispersive spectroscopy (EDS) mapping of the prepared samples was taken using a field-SEM (G360, Carl Zeiss AG, Germany).

2.4.2. Transmission Electron Microscopy (TEM). Copper grids were mounted on the surface of the collector, on which the nanofibers were directly deposited for a few seconds. TEM (Talos F200X, Thermo Scientific) was employed to observe the morphology and size of the synthesized Ag NPs in the PA56/Ag nanofibers.

2.4.3. Fourier Transform Infrared (FTIR) Spectroscopy. The FTIR spectra of the PA56/Ag nanofiber meshes in the infrared region were recorded in attenuated total reflection (ATR) mode within the spectral range of 4000−400 cm^{-1} at a resolution of 4 cm^{-1} (V70, Bruker, Germany).

2.4.4. X-ray Photoelectron Spectroscopy (XPS). The surface chemistry of the PA56/Ag nanofibrous mats was analyzed by a PHI-5000C ESCA system (PerkinElmer) with Al Kα radiation ($h\nu$ = 1486.6 eV). Carbon at 284.5 eV was used as a reference to correct for the charge effects. Both survey spectra (from 0 to 1200 eV) and high-resolution spectra with a high resolution of 0.1 eV were recorded.

2.4.5. X-ray Diffraction (XRD). The crystal structure of Ag NPs incorporated in nanofibers was analyzed by an XRD technique (D8 ADVANCE, Bruker, Germany). The intensity data of diffraction peaks were measured using Cu Kα radiation at a voltage of 40 kV and a current of 30 mA. The 2θ range was set from 10 to 90° with a 0.01° step, and each step had an exposure time of 1 s.

2.4.6. Differential Scanning Calorimetry (DSC). The melting behaviors of neat PA56 and PA56/Ag nanofibers were evaluated by using DSC (Q20, TA Instruments). The measurements were carried out from room temperature to 300 °C with a heating rate of 10 °C/min under a nitrogen atmosphere. Samples of approximately 5 mg were loaded for each measurement. The crystallinity, X_c (%), for each sample could be calculated by $X_c = \Delta H_m/\Delta H^\circ \times 100\%$, where ΔH_m is the melting enthalpy and ΔH° is the melting enthalpy of 100% crystal.

2.4.7. Universal Testing. The mechanical properties of neat PA56 and PA56/Ag nanofibers were examined by uniaxial tensile testing (PY-H801, Puyun Electronic, China). The dried membranes were cut into 10 × 100 mm^2 rectangles with a thickness between 100 and 150 μm. Samples were connected vertically between the two jaws of the tester, the gage length was adjusted to 60 mm, and the gage width was set to 10 mm. Tensile tests were evaluated at a speed of 50 mm/min. The representative tensile stress−strain curves were recorded, and the tensile strength, elongation at break, and Young's modulus of all types of nanofibers were determined.

2.4.8. Water Contact Angle (WCA). The wettability of PA56/Ag nanofibers was determined with a drop shape analyzer (DSA100, KRUSS Scientific, Germany) by the sessile drop method. The measurements were made by dispensing a 2 μL droplet on the surface of PA56/Ag nanofibrous mats with three determinations.

2.5. Antimicrobial Activity of PA56/Ag Nanofibers. The antimicrobial activity was evaluated against the *S. aureus* and *E. coli* strains. For the zone of inhibition test, circular disks with a diameter of 6 mm were punched out from the nanofiber meshes and disinfected with 1 h of UV radiation. LB agar plates were prepared and inoculated with 100 μL of bacterial solution (1 × 10^8 CFU/mL). Subsequently, the prepared disks with various Ag NP contents (0.1, 0.2, and 0.4 wt %) were placed firmly on the surface of each plate. After incubation for 24 h at 37 °C, images were captured and the inhibition zone diameter was determined by ImageJ software. The PA56-only disks were also prepared as a control group. Moreover, part of these samples was used to perform the inhibition zone assay directly, and the others were conducted to explore the impact of repeated exposure 3 or 10 times. Thus, the halo inhibition was compared before and after the repeated exposure to verify if the antibacterial activity was maintained.[10]

For quantitative antibacterial analysis, PA56/Ag nanofibers were sterilized and cut into pieces (approximately 40 mg), which were then placed in a 24-well plate. The *S. aureus* and *E. coli* cultures were diluted to a concentration of 1 × 10^5 CFU/mL. Then, 2 mL of bacterial suspension was added to each well, covering the PA56/Ag nanofiber meshes. After 24 h of incubation at 37 °C, the bacterial suspensions were smeared onto LB plates. The number of colonies in different groups was counted after 24 h of culture.[22]

2.6. In Vitro Biocompatibility of PA56/Ag Nanofibers. For cytotoxicity assay, PA56/Ag nanofiber meshes were immersed in DMEM for 24 h to obtain extracting solution with a concentration of 2 mg/mL. Then, 3T3 cells were seeded in 96-well plates (1 × 10^4 cells) and maintained overnight, followed by incubation with extracting solutions for 24 and 48 h. Afterward, 10 μL of CCK-8 reagent was added to each well and incubated at 37 °C for 1 h. The absorbance of each well at 450 nm was obtained by a microplate reader (Varioskan LUX, Thermo Scientific), and cell viability was calculated as follows: Cell viability (%) = $(A_{sample} - A_{blank})/(A_{control} - A_{blank}) \times 100\%$.

2.7. Skin Stimulation Test. To evaluate the potential skin inflammation caused by PA56/Ag nanofibers, the samples were placed on the back skin of mice. After coating with gauze and plastic film, they were secured using a bandage for 24 h. Representative images for each condition were imaged after application. Then, the applied skin was excised, stained with hematoxylin and eosin (H&E), and imaged under a microscope.[23] The back skin was shaved with electric clippers, and a depilatory cream was applied 24 h prior to the experiment. All skin test experiments were approved by the Jiaxing University Ethics Committee and carried out in accordance with the

https://doi.org/10.1021/acsomega.4c00176
ACS Omega 2024, 9, 19272−19281

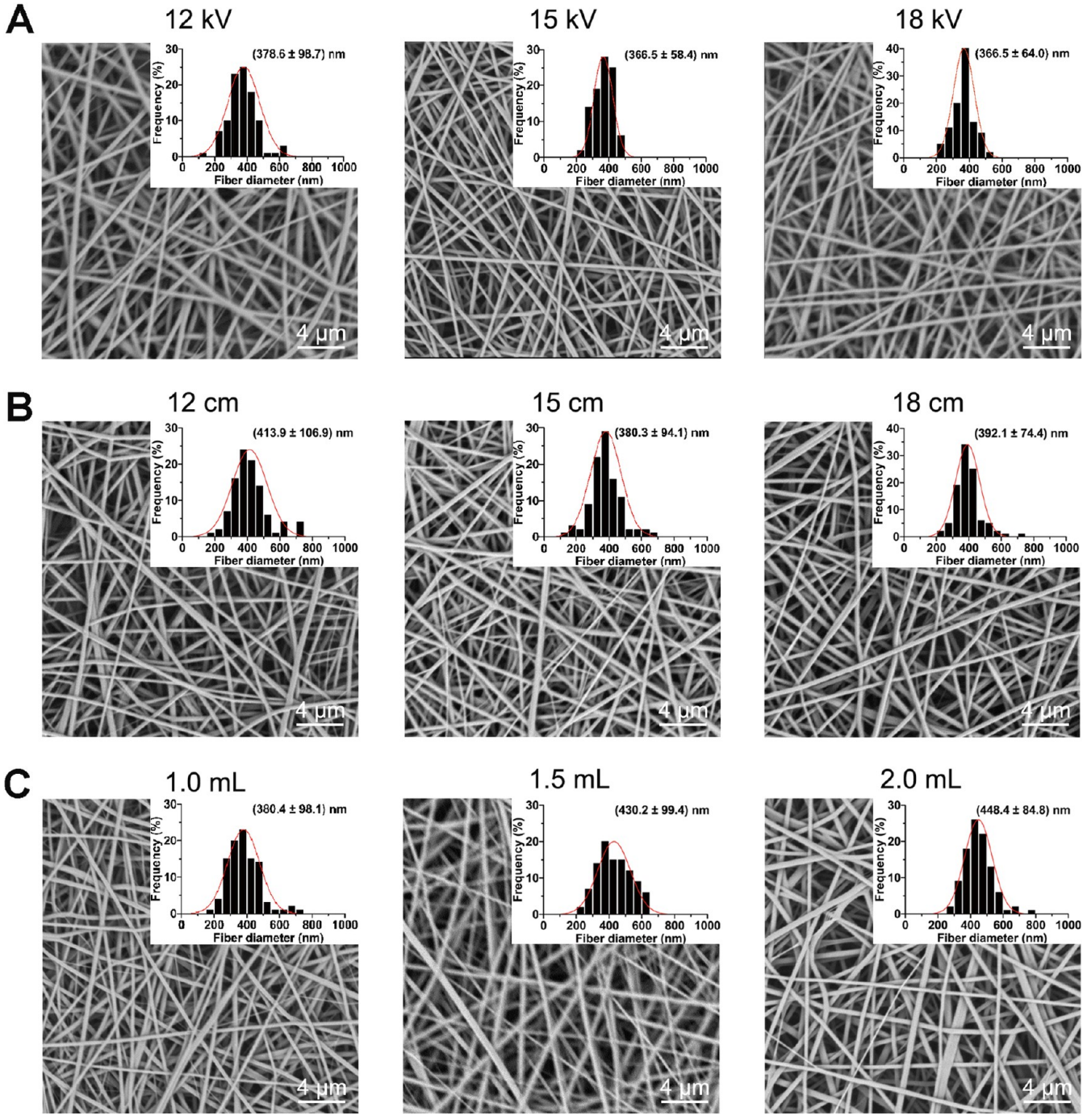

Figure 2. SEM images and diameter distribution of PA56 nanofibers under different (A) voltages, (B) collecting distances, and (C) flow rates. Scale bar = 4 μm.

National Institute of Health Guide for the Care and Use of Laboratory Animals.

2.8. Statistical Analysis. All of the data are presented as mean ± standard deviation (SD). One-way ANOVA was used for multiple comparisons when more than two groups were compared, while the two-tailed Student's t test was used for two-group comparisons. Statistical significance is indicated as $^{*}P < 0.05$, $^{**}P < 0.01$, $^{***}P < 0.001$, and $^{****}P < 0.0001$.

3. RESULTS AND DISCUSSION

3.1. Electrospinning of PA56 Nanofibers. The formation of biobased PA56 nanofibers and control of their diameters were determined by the processing parameters, including the applied voltage, the flow rate of liquid, and the distance between the spinneret and collector.[9,20] As displayed in the SEM analysis, the PA56 nanofibers at a low voltage of 12 kV exhibited undesirable morphology with an average diameter of 378.6 ± 98.7 nm (Figure 2A). An enhanced voltage led to a decrease in diameter, and nanofibers fabricated at 15 kV had an average diameter of 366.5 ± 58.4 nm. Previous studies have emphasized the critical role of higher voltages in fabricating PA56 nanofibers due to their viscosity and thermal properties.[24] In this study, HFIP replaced HCOOH in the preparation process, which significantly reduced the applied

https://doi.org/10.1021/acsomega.4c00176
ACS Omega 2024, 9, 19272−19281

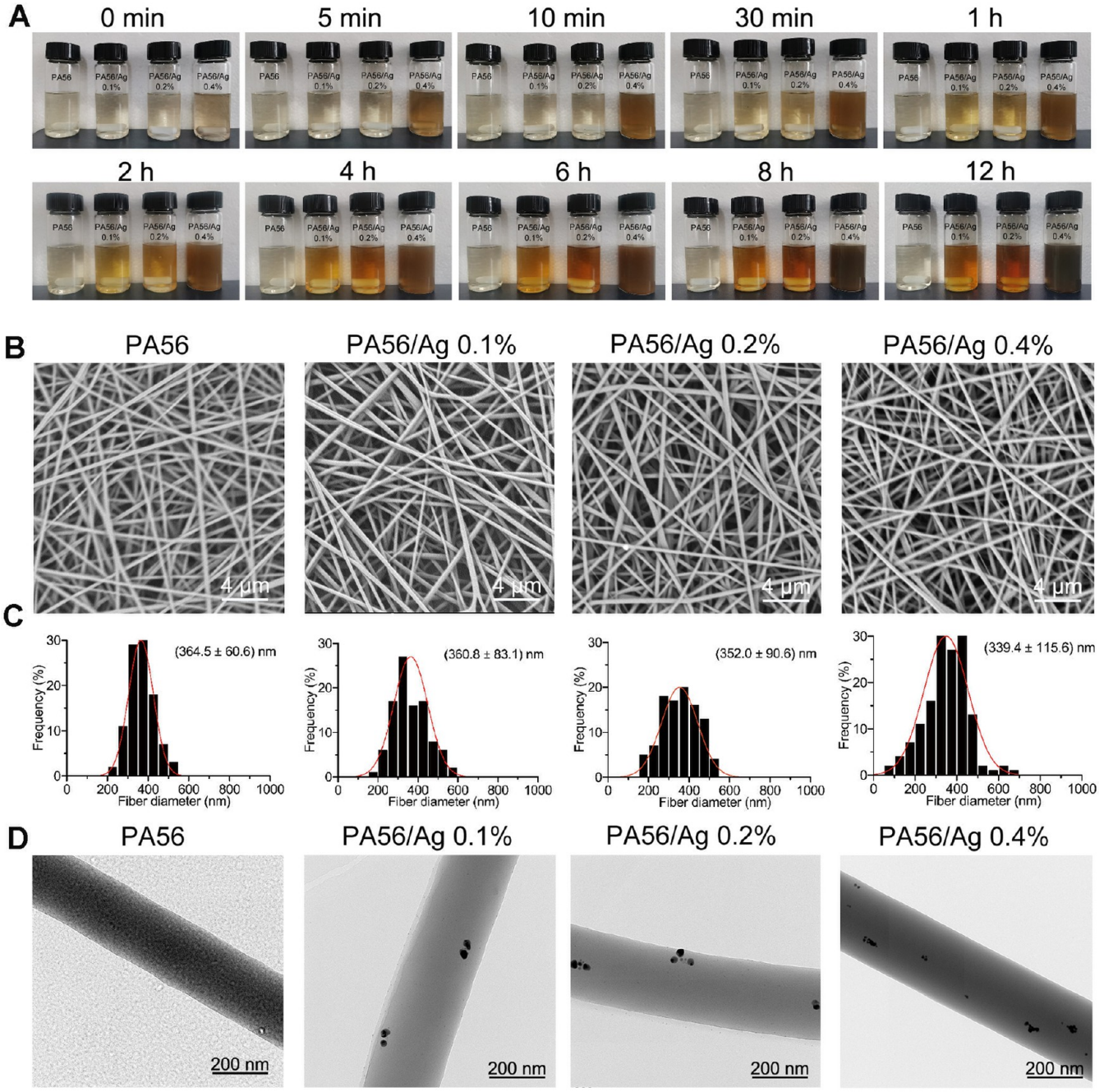

Figure 3. (A) Optical images showing the formation of Ag NPs. (B) SEM images and (C) diameter distribution for PA56, PA56/Ag 0.1%, PA56/Ag 0.2%, and PA56/Ag 0.4% nanofibers. Scale bar = 4 μm. (D) TEM images for PA56, PA56/Ag 0.1%, PA56/Ag 0.2%, and PA56/Ag 0.4% nanofibers. Scale bar = 200 nm.

voltage. By shortening the distance between the spinneret and collector, the work distance of 12 cm resulted in a higher diameter of 413.9 ± 106.9 nm, while that of 15 cm resulted in a higher diameter of only 380.3 ± 94.1 nm (Figure 2B). Regarding the flow rate, any increase would typically result in the formation of nanofibers with enlarged diameters (Figure 2C). The diameter increased from 380.4 ± 98.1 nm at 1.0 mL/h to 448.4 ± 84.8 nm at 2.0 mL/h. In general, the morphology and diameter of PA56 nanofibers were controlled by the intricate interplay of all of the processing parameters. Eventually, a solution of 12% (w/v) PA56 under 15 kV, with a flow rate of 1 mL/h and a distance of 15 cm between the needle and collector, was used to generate bead-free and uniform PA56 nanofibers.

3.2. Fabrication of Ag NPs and PA56/Ag Nanofibers.

We prepared colloidal Ag NPs stabilized with PA56 by the modified Tollens' process using HCOOH as the reducing agent. In this process, silver acetate was dissolved in aqueous ammonium hydroxide to form reactive silver ammonia complex, without silver oxide intermediate.[21] The reactive complex was then mixed with a PA56/HFIP solution, and HCOOH was titrated into the solution under stirring. The excess ammonia preferentially complexed with HCOOH, leading to the in situ synthesis of ammonium formate. With time going on, part of the labile ammonia ligands evaporated,

https://doi.org/10.1021/acsomega.4c00176
ACS Omega 2024, 9, 19272−19281

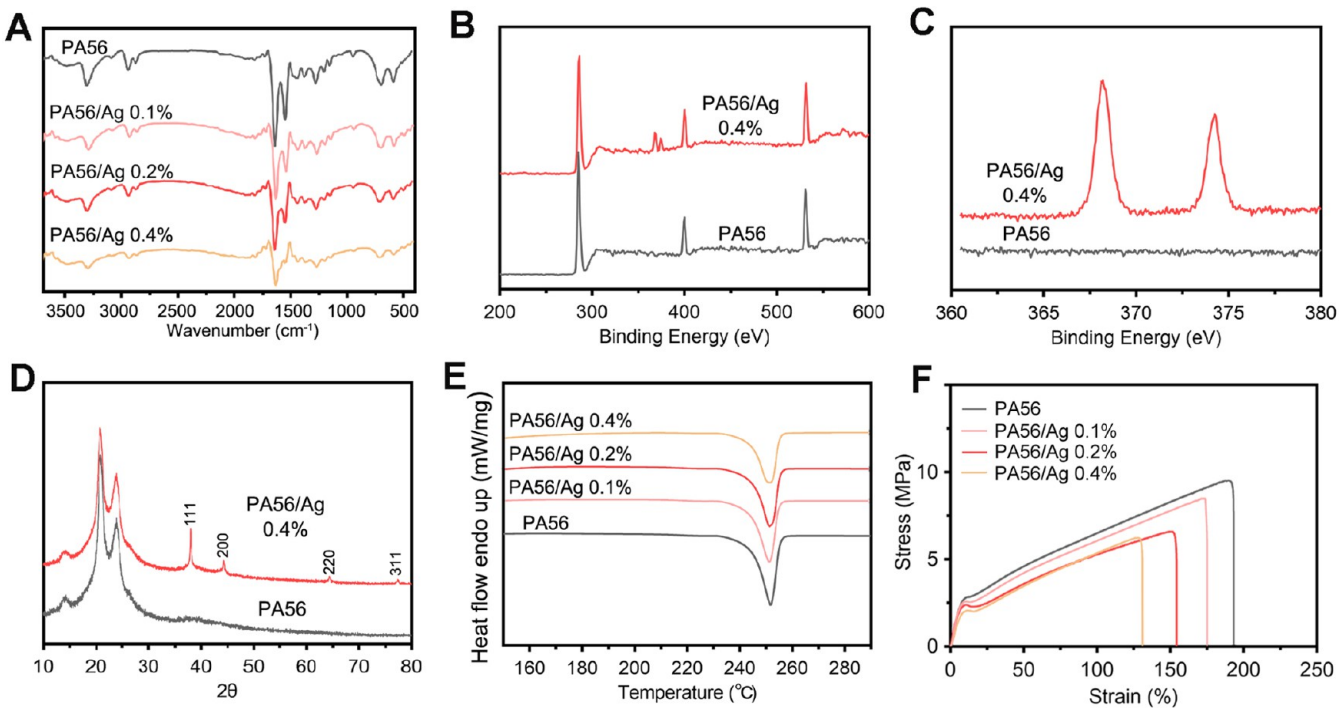

Figure 4. (A) FTIR spectra of PA56 and PA56/Ag nanofibers. (B) XPS survey spectra and (C) Ag 3d high-resolution spectra of PA56 and PA56/Ag nanofibers. (D) XRD patterns of PA56 and PA56/Ag nanofibers. (E) DSC curves and (F) representative tensile stress−strain curves of PA56 and PA56/Ag nanofibers.

allowing the reduction of silver cations by formate anions.[21] Therefore, the solution changed from colorless to bright yellow in color, and a reddish-brown was observed when the Ag concentration reached 0.4 wt % (Figure 3A).[25] During the electrospinning process, ammonia ligands and low-boiling-point reactants quickly evaporated, resulting in the complete form of Ag NPs and solid nanofibers on the collector. The difference between our Ag NPs and those prepared in the previous work lay in the choice of reducing and stabilizing agents. The use of HCOOH led to the formation of carbon dioxide and water, leaving no residual reducing agent. Additionally, we were able to introduce a low concentration of reducing agents by using HFIP instead of HCOOH, enabling a controlled environment for the in situ generation of Ag NPs. Furthermore, PA56 polymers were used to prevent Ag NPs from agglomeration, presumably because of the weak bonds between ions or Ag NPs with the NH group and the CO group of the PA56 stabilizing agent.

Among these, blank PA56 nanofibers exhibited uniform morphology and smooth surface, with an average diameter of 364.5 ± 60.6 nm, while that with 0.4% Ag NPs demonstrated the smallest fiber diameter of 339.4 ± 115.6 nm (Figure 3B,C). The growing charge density of solution gave a strong elongation force to the ejected polymeric jet, leading to smaller diameters.[9] Surface examination revealed smooth and regular nanofibers without agglomerated Ag NPs, but EDS mapping showed that Ag NPs were dispersed homogeneously in the prepared samples (Figure S1). Furthermore, the formation and size distribution of Ag NPs within nanofibers were characterized by TEM. The results showed that the in situ synthesized Ag NPs were distributed uniformly with an average size of approximately 32.4 nm, which were reported to show higher antimicrobial efficacy (Figure 3D).[26] We inferred that most of the Ag existed in the form of reactive silver ammonia complex, while Ag NPs incorporated in solid PA56 nanofibers were fabricated during electrospinning. Conversely, the synthesized Ag NPs were not dispersed effectively in solution through ultrasonication, which easily formed droplets or agglomerations within fibers.[27]

3.3. Chemical Composition of PA56 and PA56/Ag Nanofibers. FTIR analysis was conducted to confirm the presence of functional groups in the PA56 nanofibers (Figure 4A). The broad band at 3305 cm^{-1} was related to N−H stretching vibration, while the peaks at 2930 and 2864 cm^{-1} represented asymmetric and symmetric $-CH_2$ stretching, respectively. The characteristic peaks of amide I (C═O) and amide I (N−H) are located at 1631 and 1541 cm^{-1}, respectively. These bands corresponding to the functional groups of PA56 were present in all nanofibers.[5,8] For PA56/Ag nanofibers, all of the samples showed a vibration around 500 cm^{-1} corresponding to Ag−O, representing the existence of Ag NPs.[28]

XPS spectra were measured to verify the in situ production of Ag NPs in nanofibers. The existence of C, N, and O elements was validated in PA56, with peaks at 284.7, 402.8, and 534.0 eV, respectively (Figure 4B).[29] The high-resolution XPS spectrum exhibited doublet peaks at 368.2 and 374.2 eV, corresponding to the binding energy of Ag $3d_{5/2}$ and Ag $3d_{3/2}$ (Figure 4C). The gap of 6.0 eV between core levels indicated the oxidized species of Ag.[25]

XRD technique was utilized to observe the impregnation of Ag NPs in PA56 nanofibers, as described in the literature. The diffractograms revealed two strong peaks located at 2θ = 21 and 23°, indicating the presence of γ crystalline form from PA56 (Figure 4D).[30,31] The peaks for PA56/Ag nanofibers were located in the range of 38.1, 44.3, 64.3, and 77.4°, attributed to the diffraction of (111), (200), (220), and (311) crystalline planes of the face-centered structure of Ag (JCPDC

https://doi.org/10.1021/acsomega.4c00176
ACS Omega 2024, 9, 19272−19281

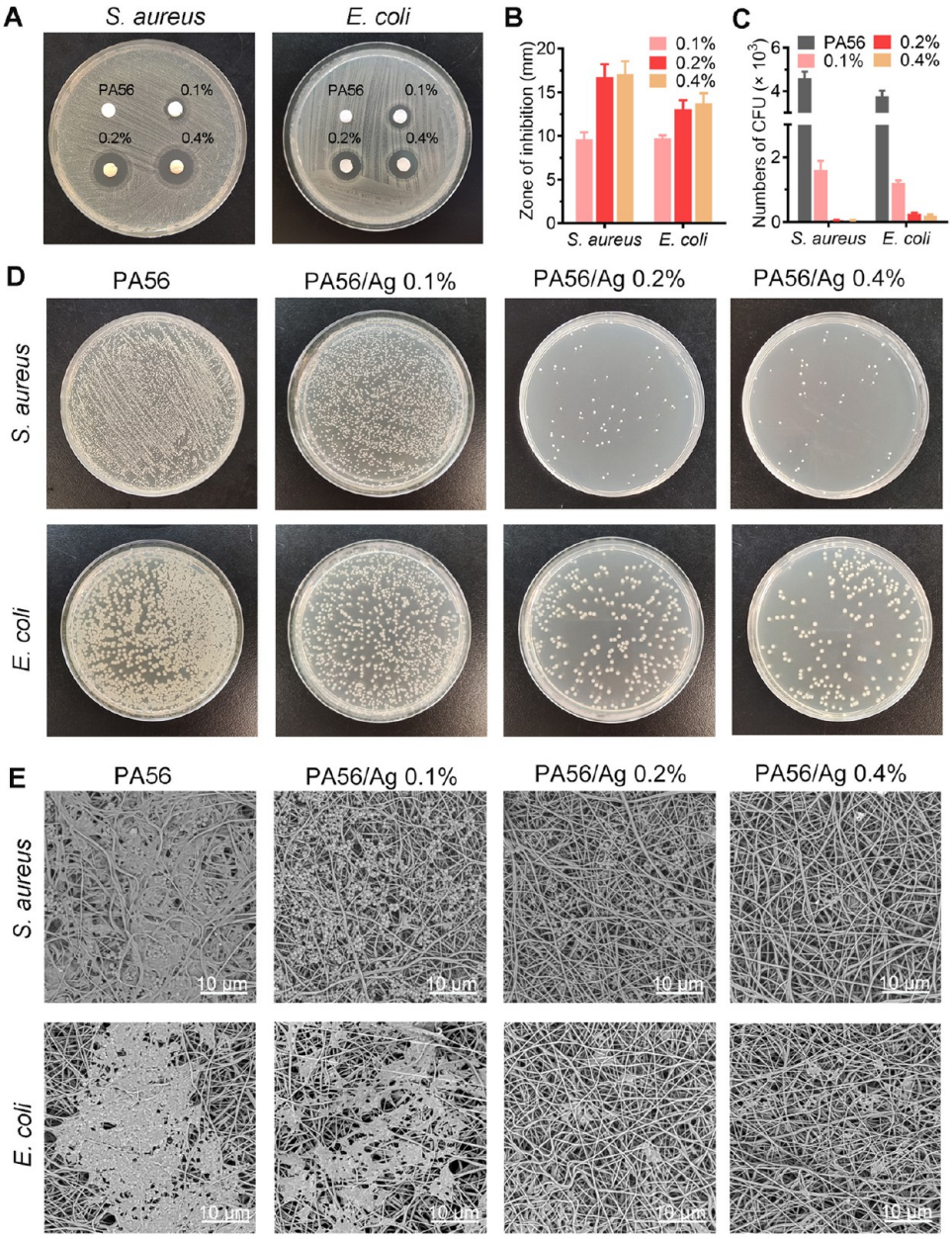

Figure 5. In vitro antibacterial activity of PA56/Ag nanofibers. (A) Photos of disk diffusion test with PA56/Ag nanofibers containing 0%, 0.1%, 0.2%, and 0.4% contents of Ag NPs. (B) The corresponding radius of the zone of inhibition. (C) Numbers of colony forming units (CFU) counted. (D) Photos of *S. aureus* and *E. coli* with PA56/Ag nanofibers containing 0, 0.1, 0.2, and 0.4% contents of Ag NPs. (E) SEM images for morphological changes of *S. aureus* and *E. coli* on PA56/Ag nanofibers.

NO. 04−0783), respectively. There was no peak for silver acetate or HFIP, suggesting that the residual acetate groups and solvents were removed by electrospinning.

The DSC curve of PA56 nanofibers exhibited a melting endothermic peak at approximately 252 °C, consistent with previous studies (Figure 4E).[8,32] The addition of Ag NPs in PA56 nanofibers had no significant influence on melting temperature, while the melting peak area decreased with increasing Ag NPs content. Here, the value of ΔH° for PA56 crystal was 188.7 J/g;[33] thus, the resulting X_c values for PA56, PA56/Ag 0.1%, PA56/Ag 0.2%, and PA56/Ag 0.4% nanofibers were 35.8, 30.4, 28.5, and 26.9%, respectively. It was observed that the crystallinity of nanofibers decreased with an increasing Ag NP content. This change was presumably attributed to the diminished hydrogen bonding between the molecular chains of PA56 macromolecules, caused by the presence of small-molecule substances, such as HCOOH, ammonium, and the silver ammonia complex.

3.4. Mechanical Characteristics of PA56 and PA56/Ag Nanofibers. The tensile stress−strain curves of PA56/Ag nanofibers were evaluated from force−displacement functions. It could be observed that the blank PA56 nanofibers presented an ultimate tensile strength (UTS) of 8.8 ± 0.6 MPa and that fell to 6.1 ± 0.2 MPa with increasing Ag NPs to 0.4% (Figure 4F). As well known, a higher degree of crystallinity indicates a greater number of macromolecular chain segments being incorporated into the crystalline region, thereby enhancing deformation resistance.[4,34] Therefore, it was conceivable that PA56/Ag nanofibers exhibited a lower tensile strength. Moreover, the neat sample presented the highest tensile strain

https://doi.org/10.1021/acsomega.4c00176
ACS Omega 2024, 9, 19272−19281

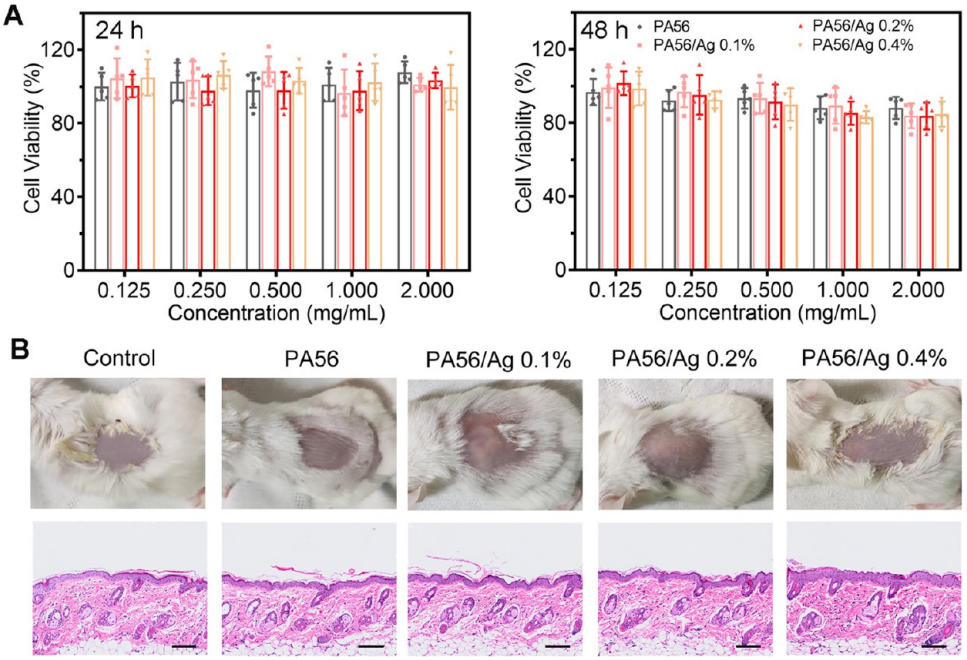

Figure 6. (A) Cell proliferation with different extracting solutions for 24 and 48 h. Data are represented as mean ± SD (n = 5). (B) Representative photos and H&E staining of application sites from each group. Scale bar = 100 μm.

at 196.8 ± 25.3%, while PA56/Ag meshes appeared to be stiffer with elongation at break at 178.7 ± 35.3, 141.2 ± 7.9, and 136.0 ± 11.4%, respectively (Table S1). The Young's modulus of PA56 nanofibers was 3.7 ± 0.7 MPa, similar to that of PA56/Ag. Collectively, the mechanical properties of PA56 nanofibers were in agreement with those of previously published work.

3.5. Contact Angle Analysis of PA56 and PA56/Ag Nanofibers. The wettability of the nanofibers was assessed through WCA analysis. Figure S2 visually illustrates the differences in WCA between PA56 and PA56/Ag nanofibers. The surface WCA of PA56 nanofibers approached approximately 78°, and the water droplet immersed through the membrane quickly within 1 s, implying the surface wetting behavior of PA56 nanofibers.[35] It is known that PA polymers have certain hydrophilicity due to the repeating units of polar amide groups (−CONH−) along the polymer chains. When Ag NPs were incorporated into nanofibers, no significant changes in WCA values were observed as the content of Ag NPs increased, while the water drop disappeared within 2 s. The reason for these results might be attributed to the morphology of nanofibrous mats, which played a pivotal role in water wettability.

3.6. In Vitro Antibacterial Evaluation of PA56/Ag Nanofibers. The antimicrobial activity of PA56/Ag nanofibers was investigated against Gram-positive *S. aureus* and Gram-negative *E. coli*. The formation of inhibition zones in agar diffusion plate tests was observed, as displayed in Figure 5A.[10] The PA56-only mats did not offer any antibacterial activity for either strain, whereas PA56/Ag containing 0.2 and 0.4% Ag NPs showed the strongest inhibition zones, with a diameter of approximately 15 mm against *S. aureus*, which was higher than that of the 0.1% group (Figure 5B). For *E. coli* bacteria, PA56/Ag nanofibers also presented clear zones of inhibition, with the 0.2 and 0.4% groups displaying better antibacterial activity than that of 0.1%. The antibacterial behaviors of PA56/Ag mats were more pronounced for *S. aureus* that is a Gram-positive strain compared to the Gram-negative *E. coli* strain, in agreement with the literature.[14] Moreover, the antibacterial results also demonstrated the presence of inhibition zones before and after ten exposures (Figure S3).

To quantify the antibacterial properties of PA56/Ag nanofibers, a standard plate counting approach that tracked bacterial proliferation was performed. After incubation with the bacterial suspension, *S. aureus* and *E. coli* in PA56/Ag nanofiber groups showed lower viability than those in the PA56 groups, where bacterial colonies proliferated extensively (Figure 5C,D). Increasing the content of Ag NPs in nanofibers significantly enhanced their antibacterial capability against both *S. aureus* and *E. coli*. The PA56/Ag 0.1% exhibited better antibacterial activity against *S. aureus* (68.0 ± 1.8%) than *E. coli* (64.9 ± 5.0%). At a mass fraction of 0.2% Ag NPs, a sharp decrease in colony formation occurred. The PA56/Ag containing 0.2 and 0.4% contents of Ag NPs effectively suppressed the bacteria growth, and the bacterial inhibition rate of PA56/Ag 0.2% was 98.7 ± 0.2% for *S. aureus* and 93.3 ± 0.9% for *E. coli*.

Furthermore, the SEM micrographs in Figure 5E compared the PA56-only nanofibers with the PA56/Ag nanofibers, revealing distinct differences in the morphology and membrane integrity of healthy and dead bacteria upon exposure to nanofibrous mats. The bacteria in pure PA56 group exhibited normal morphology, while bacteria on the surface of PA56/Ag nanofibers displayed wrinkled and distorted cell membranes, indicating the damage caused by Ag NPs. Collectively, PA56/Ag nanofibers would work as powerful antibacterial materials.

3.7. In Vitro Biocompatibility of PA56/Ag Nanofibers. The 3T3 cells were incubated with extracting solution to check the biosafety of the materials used to fabricate the PA56/Ag nanofibers. As displayed in Figure 6A, all of the groups maintained cell viability over 95% after 24 h and 85% after 48 h according to the CCK-8 assay. There were no statistically significant differences in cell proliferation among the PA56,

https://doi.org/10.1021/acsomega.4c00176
ACS Omega 2024, 9, 19272−19281

0.1, 0.2, and 0.4% PA56/Ag groups at various time points. These findings suggested that the proposed PA56/Ag nanofibers were suitable for biomedical applications and functional textiles.

3.8. Assessment of Skin Stimulation. Micrographs of the skin surface at different time points after PA56 or PA56/Ag application are depicted in Figure 6B. No evidence of erythema, edema, or other changes was found on the skin surface after patch application for 24 h. Moreover, there was inconspicuous local inflammation or adverse events in viable epidermis and dermis, suggesting that the antibacterial PA56/Ag nanofibers were biocompatible and well tolerated by skin.[23]

4. CONCLUSIONS

Embedded Ag NPs within nanofibers represent a highly promising alternative to common antimicrobial materials, but it is limited by the aggregation problem and complex deposition procedure of Ag NPs. In this study, we developed a novel one-step route to fabricate PA56 nanofibers homogeneously embedded with Ag NPs, without the need for ultrasonic dispersion or complex post-treatment. Characterization assays such as SEM, TEM, FTIR, XPS, XRD, and DSC confirmed the successful impregnation of Ag NPs. The PA56/Ag nanofibers also displayed suitable morphology, mechanical properties, and good biocompatibility in vitro. Moreover, the designed PA56/Ag possessed excellent antibacterial properties against *S. aureus* and *E. coli*. On the basis of these results, we proposed PA56/Ag as a novel antimicrobial material for potential applications in biomedical areas.

■ ASSOCIATED CONTENT

Supporting Information

The Supporting Information is available free of charge at https://pubs.acs.org/doi/10.1021/acsomega.4c00176.

EDS mapping; WCA analysis; disk diffusion tests; and mechanical properties of PA56/Ag nanofibers (PDF)

■ AUTHOR INFORMATION

Corresponding Author

Wei Wang − *College of Materials and Textile Engineering, Jiaxing University, Jiaxing 314001, China*; Email: zjxuwangwei@163.com

Authors

Zhen Wang − *The First Hospital of Jiaxing, First Affiliated Hospital of Jiaxing University, Jiaxing 314001, China*; orcid.org/0009-0000-7161-8658

Qing Gao − *The First Hospital of Jiaxing, First Affiliated Hospital of Jiaxing University, Jiaxing 314001, China*

Bailong Hou − *The First Hospital of Jiaxing, First Affiliated Hospital of Jiaxing University, Jiaxing 314001, China*

Wei Wang − *The First Hospital of Jiaxing, First Affiliated Hospital of Jiaxing University, Jiaxing 314001, China*

Liya Xu − *College of Materials and Textile Engineering, Jiaxing University, Jiaxing 314001, China; Zhe Jiang TaiHua New Material Co., Ltd., Jiaxing 314001, China*

Complete contact information is available at: https://pubs.acs.org/10.1021/acsomega.4c00176

Author Contributions

Z.W.: data curation, visualization, validation, writing—original draft, funding acquisition. Q.G.: methodology, formal analysis. B.H.: methodology, supervision. W.W.: investigation. L.X.: project administration, funding acquisition. W.W.*: writing—review and editing, supervision, project administration, funding acquisition.

Funding

This work was supported by "Pioneer" and "Leading Goose" R&D Program of Zhejiang (2023C01201), Zhejiang Provincial Natural Science Foundation of China (LQ24H300002), Jiaxing Science and Technology Planning Project (2023AY11012), and Jiaxing Key Discipline of Medicine—Clinical Pharmacy (2023-ZC-008).

Notes

The authors declare no competing financial interest.

■ ACKNOWLEDGMENTS

This work was supported by "Pioneer" and "Leading Goose" R&D Program of Zhejiang (2023C01201), Zhejiang Provincial Natural Science Foundation of China (LQ24H300002), Jiaxing Science and Technology Planning Project (2023AY11012), and Jiaxing Key Discipline of Medicine—Clinical Pharmacy (2023-ZC-008).

■ REFERENCES

(1) Varghese, M.; Grinstaff, M. W. Beyond nylon 6: polyamides via ring opening polymerization of designer lactam monomers for biomedical applications. *Chem. Soc. Rev.* **2022**, *51* (19), 8258−8275.

(2) Lee, Y.; Andrew Lin, K.-Y.; Kwon, E. E.; Lee, J. Renewable routes to monomeric precursors of nylon 66 and nylon 6 from food waste. *J. Cleaner Prod.* **2019**, *227*, 624−633.

(3) Xu, Y.; Wang, J.; Wang, Z.; Zhao, Y.; Guo, W. Bio-based polyamide fibers prepared by mussel biomimetic modification of hydroxyapatite. *Eur. Polym. J.* **2023**, *187*, No. 111913, DOI: 10.1016/j.eurpolymj.2023.111913.

(4) Haoyu, Y.; Xiaoqi, Z.; Yiming, L.; Lu, M.; Suqin, H.; Miaoming, H.; Hao, L.; Wanlin, X.; Wentao, L. Synthesis and comprehensive characterization of bio-based polyamide 56/6 Copolymer: Mechanical, Thermal, and processing properties. *Eur. Polym. J.* **2024**, *202*, No. 112593.

(5) Kang, H.; Wang, Z.; Hao, X.; Liu, R. Thermal induced crystalline transition of bio-based polyamide 56. *Polymer* **2022**, *242*, No. 124540, DOI: 10.1016/j.polymer.2022.124540.

(6) Yan, Y.; Gooneie, A.; Ye, H.; Deng, L.; Qiu, Z.; Reifler, F. A.; Hufenus, R. Morphology and Crystallization of Biobased Polyamide 56 Blended with Polyethylene Terephthalate. *Macromol. Mater. Eng.* **2018**, *303* (9), No. 1800214.

(7) Luzi, F.; Torre, L.; Kenny, J.; Puglia, D. Bio- and Fossil-Based Polymeric Blends and Nanocomposites for Packaging: Structure−Property Relationship. *Materials* **2019**, *12* (3), No. 471, DOI: 10.3390/ma12030471.

(8) Xue, C.; Hsu, K.-M.; Chiu, C.-Y.; Chang, Y.-K.; Ng, I. S. Fabrication of bio-based polyamide 56 and antibacterial nanofiber membrane from cadaverine. *Chemosphere* **2021**, *266*, No. 128967.

(9) Xue, J.; Wu, T.; Dai, Y.; Xia, Y. Electrospinning and Electrospun Nanofibers: Methods, Materials, and Applications. *Chem. Rev.* **2019**, *119* (8), 5298−5415.

(10) Garcia, M. M.; da Silva, B. L.; Sorrechia, R.; Pietro, R. C. L. R.; Chiavacci, L. A. Sustainable Antibacterial Activity of Polyamide Fabrics Containing ZnO Nanoparticles. *ACS Appl. Bio Mater.* **2022**, *5* (8), 3667−3677.

(11) Dizaj, S. M.; Sharifi, S.; Jahangiri, A. Electrospun nanofibers as versatile platform in antimicrobial delivery: current state and perspectives. *Pharm. Dev. Technol.* **2019**, *24* (10), 1187−1199, DOI: 10.1080/10837450.2019.1656238.

(12) Alzahrani, S. O.; Al-Ghamdi, S. A.; Alsahag, M.; Alatawi, K.; Alaysuy, O.; Al-Ahmed, Z. A.; El-Metwaly, N. M. Nanosilver-doped carbon quantum dots for industrialization of efficacious textiles with

superior UV-resistance and antimicrobial performance. *Diamond Relat. Mater.* **2023**, *138*, No. 110249.
(13) Snari, R. M.; Alzahrani, S. O.; Katouah, H. A.; Alkhamis, K.; Alaysuy, O.; Abumelha, H. M.; El-Metwaly, N. M. Optical properties of novel luminescent nacre-like epoxy/graphene nanocomposite coating integrated with lanthanide-activated aluminate nanoparticles. *Luminescence* **2022**, *37* (9), 1482−1491.
(14) Xie, X.; Sun, T.; Xue, J.; Miao, Z.; Yan, X.; Fang, W.; Li, Q.; Tang, R.; Lu, Y.; Tang, L.; Zha, Z.; He, T. Ag Nanoparticles Cluster with pH-Triggered Reassembly in Targeting Antimicrobial Applications. *Adv. Funct. Mater.* **2020**, *30* (17), No. 2000511, DOI: 10.1002/adfm.202000511.
(15) Haidari, H.; Bright, R.; Strudwick, X. L.; Garg, S.; Vasilev, K.; Cowin, A. J.; Kopecki, Z. Multifunctional ultrasmall AgNP hydrogel accelerates healing of *S. aureus* infected wounds. *Acta Biomater.* **2021**, *128*, 420−434.
(16) Rafique, M.; Sadaf, I.; Rafique, M. S.; Tahir, M. B. A review on green synthesis of silver nanoparticles and their applications. *Artif. Cells, Nanomed., Biotechnol.* **2017**, *45* (7), 1272−1291.
(17) Aljohani, M.; Alkabli, J.; Abualnaja, M. M.; Alrefaei, A. F.; Almehmadi, S. J.; Mahmoud, M. H. H.; El-Metwaly, N. M. Electrospun AgNPs-polylactate nanofibers and their antimicrobial applications. *React. Funct. Polym.* **2021**, *167*, No. 104999, DOI: 10.1016/j.reactfunctpolym.2021.104999.
(18) Çimen, C. G.; Dundar, M. A.; Kars, M. D.; Avci, A. Enhancement of PCL/PLA Electrospun Nanocomposite Fibers Comprising Silver Nanoparticles Encapsulated with Thymus Vulgaris L. Molecules for Antibacterial and Anticancer Activities. *ACS Biomater. Sci. Eng.* **2022**, *8* (9), 3717−3732, DOI: 10.1021/acsbiomaterials.2c00611.
(19) Li, Y.; Chen, Y.; Li, P.; Wang, G.; Wei, J. Controllable deposition of Ag nanoparticles on various substrates via interfacial polyphenol reduction strategy for antibacterial application. *Colloids Surf., A* **2022**, *655*, No. 130287, DOI: 10.1016/j.colsurfa.2022.130287.
(20) Mogharbel, A. T.; Ibarhiam, S. F.; Alqahtani, A. M.; Attar, R. M. S.; Alshammari, K. F.; Bamaga, M. A.; Al-Qahtani, S. D.; El-Metwaly, N. M. Plasma-assisted in-situ preparation of silver nanoparticles and polypyrrole toward superhydrophobic, antimicrobial and electrically conductive nonwoven fabrics from recycled polyester waste. *J. Ind. Eng. Chem.* **2023**, *127*, 356−364.
(21) Walker, S. B.; Lewis, J. A. Reactive Silver Inks for Patterning High-Conductivity Features at Mild Temperatures. *J. Am. Chem. Soc.* **2012**, *134* (3), 1419−1421.
(22) Dong, R.; Li, Y.; Chen, M.; Xiao, P.; Wu, Y.; Zhou, K.; Zhao, Z.; Tang, B. Z. In Situ Electrospinning of Aggregation-Induced Emission Nanofibrous Dressing for Wound Healing. *Small Methods* **2022**, *6*, No. 2101247, DOI: 10.1002/smtd.202101247.
(23) Ma, W.; Li, L.; Lin, X.; Wang, Y.; Ren, X.; Huang, T.-S. Novel ZnO/N-halamine-Mediated Multifunctional Dressings as Quick Antibacterial Agent for Biomedical Applications. *ACS Appl. Mater. Interfaces* **2019**, *11* (34), 31411−31420.
(24) Xue, C.; Hsu, K.-M.; Chiu, C.-Y.; Chang, Y.-K.; Ng, I. S. Fabrication of bio-based polyamide 56 and antibacterial nanofiber membrane from cadaverine. *Chemosphere* **2021**, *266*, No. 128967, DOI: 10.1016/j.chemosphere.2020.128967.
(25) Gobi, N.; Berly, R. In situ preparation of silver nanoparticle embedded composite nanofibrous membrane: a multi-layered biocidal air filter. *J. Polym. Bull.* **2023**, *80*, 10263−10287, DOI: 10.1007/s00289-022-04561-z.
(26) Zheng, K.; Setyawati, M. I.; Leong, D. T.; Xie, J. Antimicrobial silver nanomaterials. *Coord. Chem. Rev.* **2018**, *357*, 1−17.
(27) Avci, M. O.; Muzoglu, N.; Yilmaz, A. E.; Yarman, B. S. Antibacterial, cytotoxicity and biodegradability studies of polycaprolactone nanofibers holding green synthesized Ag nanoparticles using atropa belladonna extract. *J. Biomater. Sci. Polym. Ed.* **2022**, *33* (9), 1157−1180.
(28) Sunaryono, S.; Rachmawati, A.; Yogihati, C. I.; Susanto, H.; Taufiq, A.; Mufti, N. The effect of Ag nanoparticles in Ag/polyvinyl alcohol nanofiber composites. *Polym. Bull.* **2022**, *79* (1), 555−568.
(29) Cheng, H.; Chen, X.; Sheng, Y.; Song, M.; Sun, C.; Wang, Z.; Zhou, J.; Zhang, H.; Ding, Y. Perovskite-derived pro-photosensitizer enables sustainable photodynamic therapy in hypoxia tumors. *Chem. Eng. J.* **2023**, *468*, No. 143457, DOI: 10.1016/j.cej.2023.143457.
(30) Morales-Gámez, L.; Soto, D.; Franco, L.; Puiggalí, J. Brill transition and melt crystallization of nylon 56: An odd−even polyamide with two hydrogen-bonding directions. *Polymer* **2010**, *51* (24), 5788−5798.
(31) Puiggali, J.; Aleman, C.; Ja, S.; Franco, L. J. M. Crystal structures of nylon 5,6. A model with two hydrogen bond directions for nylons derived from odd diamines. *Macromolecules* **1998**, *31* (24), 8540−8548, DOI: 10.1021/ma971895b.
(32) Yan, Y.; Gooneie, A.; Ye, H.; Deng, L.; Qiu, Z.; Reifler, F. A.; Hufenus, R. Morphology and Crystallization of Biobased Polyamide 56 Blended with Polyethylene Terephthalate. *Macromol. Mater. Eng.* **2018**, *303* (9), No. 1800214, DOI: 10.1002/mame.201800214.
(33) Puiggalí, J.; Franco, L.; Alemán, C.; Subirana, J. A. Crystal Structures of Nylon 5,6. A Model with Two Hydrogen Bond Directions for Nylons Derived from Odd Diamines. *Macromolecules* **1998**, *31* (24), 8540−8548.
(34) Nitta, K.-h.; Odaka, K. Influence of structural organization on tensile properties in mesomorphic isotactic polypropylene. *Polymer* **2009**, *50* (16), 4080−4088.
(35) Esenoğlu, G.; Tanoğlu, M.; Barisik, M.; İplikçi, H.; Yeke, M.; Nuhoğlu, K.; Türkdoğan, C.; Martin, S.; Aktaş, E.; Dehneliler, S.; Gürbüz, A. A.; İriş, M. E. Investigating the Effects of PA66 Electrospun Nanofibers Layered within an Adhesive Composite Joint Fabricated under Autoclave Curing. *ACS Omega* **2023**, *8* (36), 32656−32666.

https://doi.org/10.1021/acsomega.4c00176
ACS Omega 2024, 9, 19272−19281